SLAC-PUB-3038
LBL-15966
January 1983
(E)

MONTE CARLO STUDIES FOR THE DESIGN OF A LEAD GLASS DRIFT CALORIMETER*

H. HIRAYAMA†, W. R. NELSON
Stanford Linear Accelerator Center
Stanford University, Stanford, California 94305

A. DEL GUERRA‡, T. MULERA, V. PEREZ-MENDEZ
Lawrence Berkeley Laboratory
University of California Berkeley, California 94720

ABSTRACT

A drift collection calorimeter having a combined radiator and field shaping structure made of lead glass tubing is described. With the aid of the EGS Monte Carlo code we show that such a device, when pressurized to 10 atmospheres, will give a resolution of $\sigma/E = 9.6\%/E^{1/2}$ provided that the shower is contained at a 99% level. Track length restriction and Landau sampling have been included in the EGS simulation. In addition, leading particle biasing and weighting techniques have been employed for the first time with EGS, with an increase in efficiency of about 100 to 300 for 10 GeV shower containment calculations.

Submitted to Nuclear Instruments and Methods

---

* Work supported by the Department of Energy, contract DE-AC03-76SF00515.
† Permanent address: National Laboratory for High Energy Physics (KEK), Oho-machi, Tsukuba-gun, Ibaraki, Japan.
‡ Permanent address: Dipartimento di Fisica, Piazza Torricelli 2, I-56100 Pisa, Italy.

1. INTRODUCTION

A drift collection calorimeter having a combined radiator and field shaping structure made of lead glass tubing has recently been proposed [1] and studied with the help of the EGS Monte Carlo code [2]. The results given in ref. [1] were preliminary in that the Monte Carlo studies were not complete and the effect of shower leakage from the detector was not fully appreciated at that time. We present in this paper the various details of the calculation along with results that explain the gain or loss of energy resolution in terms of path length restriction, Landau fluctuations, and leakage. These effects, of course, have been observed many times elsewhere (see, for example, the reviews by Fabian and Ludlam [3] and by Iwata [4]). In particular, we have created pictures of the showers in order to graphically visualize what is happening. An additional feature of this work is a glimpse at the new methods that will shortly be available for the enhanced version of EGS called EGS4, written by two of the above authors (WRN and HH).

2. THE PROPOSED LEAD GLASS DRIFT CALORIMETER

In this design, which is an adaptation of converters used for positron emission tomography [5], tubes of high density (80% PbO) lead glass are fused together with their axes perpendicular to the direction of incident radiation as shown in fig. 1. The glass has a density of 6.3 g cm^{-3} and a radiation length of 1.3 cm. The tubes we considered had inner diameters which varied from 3 to 10 mm and wall thicknesses of 1 or 2 mm. The resistive metallic layer, which acts as a continuous voltage divider for drift field shaping, is made by reducing a surface layer of the PbO to metallic lead by heating in a hydrogen atmosphere. The procedure is described in detail elsewhere [5] and in other references therein. Typical layers have resistances of 50-200 MΩ/square

and are uniform among the tubes to within $\pm 10\%$. Scaling up the dimensions of these converters [5,6] and drawing on other authors' studies of drifting in extreme aspect ratio geometries [7-9] we believe that, with the proper choice of gas mixture, pressure, and inside tube diameter, one should be able to employ the proposed structure with drift path lengths of up to 50 cm without degradation of calorimeter performance due to electron loss.

The chemical reduction of PbO on the glass surface is a convenient method of providing a uniform resistive layer to define the potential everywhere on the surface of the drift structure. It is particularly convenient for small diameter tubes where such methods as coating uniformly with resistive inks would prove difficult. The use of such continuous electrodes to avoid field distortions due to the edges of discrete electrodes and the presence of nearby conductors is of great importance in avoiding loss of electrons while drifting in long, narrow spaces [8].

The use of tubes rather than planar drift spaces has some advantages in itself. The fused mass of tubes provides a rigid self-supporting structure and makes a more compact calorimeter. The tubular configuration gives a large surface-to-volume ratio which reduces the loss of energy trapped unseen in the radiator and the consequent degradation of resolution. Further improvement in the energy resolution is obtained from the tubes' limiting of track length variations in the direction transverse to the tube axes. This reduces the fluctuation due to the wide angular distribution of the very soft shower electrons in the sampling gap. These fluctuations have been shown to be a major contribution to the loss of resolution in gas sampling devices [10].

The wire chamber used to read out the calorimeter may be oriented with the anode wires either parallel or perpendicular to (as shown in fig. 1) the direction of the development of the shower. In the orientation shown, longitudinal segmentation is obtained by reading out individual wires, and transverse segmentation (in the vertical

direction) is obtained by digitizing the drift time using some externally supplied start signal. Segmentation in the remaining transverse direction, along the wires, can be accomplished either by charge division along the wire or delay line readout of a cathode segmented in that direction. Our thinking favors the latter method because of the delay line's superior spatial resolution and superior capability of resolving closely spaced tracks.

The wire chamber may be operated either in the standard proportional mode or in one of the modes in which the pulse height is saturated, such as the "self-quenched streamer" mode [11-13]. In the former the signal collected from each wire is proportional to the amount of energy deposited in the tubes sampled by that wire. Thus for energy measurement, the calorimeter is not troubled by many overlapping tracks in a very high energy shower, but the resolution is degraded by the Landau fluctuations in the energy deposited by each track. In the saturated modes, one uses "digital sampling" [14] in which the measured signal is proportional to the number of tracks. This eliminates the deleterious effect of Landau fluctuations but may cause the energy response of the calorimeter to saturate at high energies due to overlapping tracks being registered as single particles traversing the tubes.

3. THE MONTE CARLO PROGRAM

3.1 General Description of EGS

For the simulation of cascade showers in the detector, a general electromagnetic radiation transport code called EGS (Electron-Gamma Shower), written by Ford and Nelson [2], was used. The EGS code is written in an extended FORTRAN language known as MORTRAN [15] and is currently being used by many people to solve a variety of problems in accelerator, high-energy, medical, and health physics [16]. Probably its

most popular use of late is in the design of shower detection devices, such as calorimeters. In particular, EGS is capable of treating electrons, positrons, and photons with kinetic energies as high as 3000 GeV and as low as 1 keV (photons) and 1 MeV (electrons and positrons).* The transport can take place in any of 100 different elements, or in any mixture or compound of these elements. It is left up to the user to construct his own geometry and to score a particular answer, which has led to a vast assortment of complex simulations of late [16]. The user interacts with EGS by means of a "User Code", which is most effective when written in MORTRAN, taking advantage of the macro-facility inherent to the language.

The computational portion of the EGS Code System is divided into two parts. First, a preprocessor code (PEGS) uses theoretical (and sometimes empirical) formulas to compute the various physical quantities needed (e.g., cross sections, branching ratios, etc.) and prepares them in a form suitable for fast numerical evaluation. Then the EGS code itself uses this data, along with user supplied data and routines, to perform the actual simulation.

The EGS code consists of two "user-callable" subroutines, HATCH and SHOWER, which in turn call the other subroutines in the EGS code – some of which call two necessary "user-written" subroutines, HOWFAR and AUSGAB. The latter determine the geometry and output (i.e., scoring), respectively. The user communicates with EGS by means of various COMMON variables and the four subprograms above. To use EGS, the user must write a MAIN program and the subroutines HOWFAR and AUSGAB which, together with any user supplied subprograms, constitute the User Code for the problem at hand.

---

* The new version mentioned earlier, EGS4, is able to follow electrons down to kinetic energies of 10 keV, and this feature was included into our version of EGS3 and applied to the gas regions of the geometry (only).

3.2 UCCAL – The Lead Glass Tube Calorimeter User Code

As stated above, the user communicates with the EGS code by means of MAIN (to initialize AUSGAB/HOWFAR and to initiate events) and the subroutines HOWFAR (to specify the geometry) and AUSGAB (to score and output results). The tube geometry shown in fig. 1 presents a very difficult problem in that the HOWFAR description would be extremely complicated and difficult to code. As a result, the simulation would be very inefficient and time consuming. For situations like this it is usually best to use a simple description of the geometry and to account for the missing features, if necessary, by means of the AUSGAB routine. For the problem at hand, the tube geometry was approximated by alternating slabs of lead glass and gas regions, with the effective dimensions chosen to give the same average cross sectional area of gas and solid material when viewed from the edge of the slabs (or tubes) (see Appendix). The slabs were also taken to be infinite in the transverse directions (x and y) to the beam, which was incident normal to the slabs along the z-axis. Consequently, the HOWFAR description was extremely simplified.

Figure 2 shows tracks of charged particles (solid lines) and photons (dots) for a cascade initiated by a single 1 GeV electron. The narrow slabs correspond to PbO material and the wider ones to the gas region. In this example the (equivalent) dimensions correspond to tubes with an inner hole diameter of 10 mm filled with P30 (70% Ar, 30% CH_4) gas at NTP, and with wall thickness of 1 mm (throughout this paper we will denote such dimensions by: 10 mm/1 mm/1 atm). The total length of the detector corresponds to approximately 15 radiation lengths and, as is typical of absorbers that are this thick, energy is carried out the back mostly by photons. The same shower is given in fig. 3, but this time only the charged particles in the gas regions are shown. It is very clear from this picture that a number of tracks have

lengths that are much larger than the gap dimension, and it is these tracks that result in fluctuations and lead to a loss in energy resolution.

The track length restriction that would be imposed by the tubes in the direction transverse to the tube axes was retained by appropriately limiting the energy deposition along the track, as described elsewhere [17]. In addition to the track length restriction, a second sampling algorithm was added to AUSGAB in order to simulate Landau fluctuations in the energy deposited in the gas by the charged particles [18].

The effect of including Landau sampling and track length restriction is shown quite nicely in the following sequence of three dimensional plots where energy deposition in the gaps is given in the vertical dimension as a function of the longitudinal direction of the shower ("hole number") and the transverse direction along the hole axes ("x-axis (cm)"). Figure 4 corresponds to no Landau fluctuations and no track length restriction. Shower maximum is reached approximately 4 radiation lengths into the medium as expected. Aside from the central development of the cascade, we observe a number of little bumps superimposed on a flat plane, which correspond to track length fluctuations. Figure 5 is the identical set of shower events with the track length restriction still not applied, but with the addition of the Landau sampling algorithm. The bumps on the surface are not significantly affected by the Landau addition, probably because they correspond to long tracks, but the amplitude of the main shower development along the beam axis has decreased, and the net effect is a further loss in resolution. Figure 6 shows the result of applying the track length restriction (including Landau). The bumps have almost disappeared and the central shower development seems to have become smoother as well. The amplitude of the shower has decreased significantly because of the track length restriction (note the factor of two change in the scale), but the fluctuations have been reduced even more so and this results in a net gain in the energy resolution.

4. APPLICATION OF EGS/UCCAL TO THE DESIGN OF THE CALORIMETER

The EGS program was run for various tube diameters, wall thicknesses, and gas pressures with incident energies of 1, 2, 4, and 10 GeV. Figure 7 gives the longitudinal development of a shower initiated by 4 GeV electrons incident on 15 radiation lengths of the proposed detector (10 mm/1 mm/1 atm). For the remainder of the calculations presented in this paper, unless otherwise indicated, both the Landau sampling and track length restriction algorithms were applied. Also shown in the figure are experimental results reported by Anderson et al [19]. Their test calorimeter had a similar arrangement of radiator and gas sampling regions to that of the lead glass device. Their sampling, however, was carried out with wires inside channels ("tubes") rather than by the drift collection technique. The similarity of the EGS results to the experimental measurement provides support that the Monte Carlo technique is successfully modeling the calorimeter response.

The total energy deposited in all gas regions is plotted on an event-by-event basis in figs. 8 and 9 for incident electron energies of 1 and 10 GeV, respectively, and for a 15 radiation length detector (15 rℓ/10 mm/1 mm/1 atm). These distributions are typical of what was obtained for all geometries that were investigated, showing a reasonable symmetry at the high energies (4 to 10 GeV) and a skewed distribution at the lower energies (1 to 4 GeV). Nevertheless, the fractional energy resolution, σ/E, was obtained directly from the Monte Carlo data using the conventional formulas for the mean value and standard deviation.

In principle, the uncertainty in the energy measurement is governed by statistical fluctuations in the shower development, and the fractional energy resolution is given by $\sigma/E = \text{constant}/E^{1/2}$ (e.g., [3]). In fig. 10 we plot the resolution as a function of $E^{-1/2}$ in order to observe any deviation from the expected straight line through

the origin (15 rℓ/10 mm/1 mm/1 atm). The errors on these points were obtained by dividing the EGS runs, for each energy, into six runs of 150 to 700 incident showers each. Each data point and error bar corresponds to the mean and standard deviation of the mean for the six runs at that energy. The curves shown are one and two parameter fits of the form $\sigma/E = \alpha_1/E^{1/2}$ and $\sigma/E = \alpha_2 + \alpha_3/E^{1/2}$. In this case, and in all the other 15 radiation length geometries studied, the two-parameter prescription provides a better fit to the data and is therefore the most appropriate form to use with a counter having these dimensions. As suggested in an earlier paper [1], the deviation of the high energy points from a straight line through the origin, as expected from the usual model, can be attributed to fluctuations caused by leakage out the back of the device. We will discuss this more thoroughly later on in the paper.

The effect of varying the inner diameter of the tube (i.e., the length of gas seen by the charged particles) is shown in fig. 11 for the case of 1 GeV and for a gas pressure of 1 atmosphere. The four curves correspond to the four combinations of applying (or not) the track length restriction and Landau sampling algorithms. The actual detector situation is given by the T.R./Landau curve where it is apparent that increasing the tube diameter from 10 to 20 mm will not significantly improve the resolution. As we will see, however, increasing the gas pressure does produce a benefit.

Table I provides a summary of the results of running EGS for several 15 radiation length geometries and gas pressures. The energy resolution as a function of incident energy is presented in terms of both one and two parameter fits. The energy resolutions obtained for gas fillings at one atmosphere pressure are comparable to those claimed for existing gas sampling devices ([3] and references contained therein). As would be expected, the resolution shows a trend towards improvement as the fraction of sampling gas to radiator is increased. This improvement must be balanced against the necessary increase in longitudinal size of the device in order to provide sufficient radiator to

contain the showers. The results at higher than atmospheric pressure suggest a method of achieving very good resolution with reasonably compact structures.

5. LEAKAGE EFFECTS: CALCULATIONS AND DISCUSSION

As suggested above, the loss of resolution at 10 GeV can be attributed to leakage out the back of the 15 radiation length detector. The obvious way to demonstrate this is to increase the length of the device. In fig. 12 we present the results for both 15 and 30 radiation length detectors (10 mm/1 mm/10 atm). The 10 atmosphere gas pressure was chosen because the 15 radiation length data had shown the largest deviation from the straight line through the origin at this pressure, although the same trend was observed in the other cases as well. It is clear from this figure that the 30 radiation length results are in perfect agreement with the $E^{-1/2}$ model. The new single parameter fit to the data also gives a slightly better value for the resolution constant including a much better error [$(9.59 \pm 0.05)\%$ versus $(10.00 \pm 0.34)\%$ from table I].

In fig. 13 we plot the energy resolution as a function of the length of the detector (10 mm/1 mm/10 atm) for 1 and 10 GeV electron energies. As expected, the resolution reaches a constant value near 15 radiation lengths at 1 GeV, whereas it takes approximately 20 radiation lengths to achieve a comparable limit for the 10 GeV case. Correspondingly, in fig. 14 the resolution is plotted in terms of the fraction of energy (charged particle and photon) that leaks out the back. The arrows in the figure indicate the points that correspond to 15 and 20 radiation lengths for the 1 and 10 GeV energies, respectively. From these figures it is clear, for this type device at least, containment at the 98-99% level is required in order to obtain results that agree with the standard $E^{-1/2}$ model.

In order to see how effective the detector will be at very low energies, in fig. 15 we plot the quantity $\sigma E^{1/2}/E$ as a function of energy for both 15 and 30 radiation lengths (10 mm/1 mm/10 atm). The data is constant over the entire energy range for the 30 radiation length case and, for the 15 radiation length case, shows the expected increase after a few GeV.

6. A GENERAL (FASTER) METHOD FOR DESIGNING CALORIMETERS

The EGS code has been shown to be quite effective when used as a tool for designing calorimeters ([3] and references therein). However, EGS is inherently slow due to the fact that each and every particle in the cascade is followed until it either interacts or is discarded, putting the code in the class generally referred to as analog Monte Carlo. For the calculations presented in this paper, for example, electrons were followed down to 10 keV in the gas regions, and down to 1 MeV in the PbO regions. Photons were followed to 100 keV in all regions. The computer time required (per incident event) for the series of calculations with the 30 radiation length device (10 mm/1 mm/10 atm) is given in table II, where the event time is observed to be linear with energy. Most of the calculations below 2 GeV were from 4 to 10 minutes in length, and those above ranged from 15 to 30 minutes. As indicated earlier, this corresponded to a total number of events varying between 150 and 700 depending on the geometry that was studied. Extrapolating to 100 GeV one can easily see that it will take 2 to 3 hours in order to perform a single (80 to 125 case) run, in addition to which six or more runs are generally preferred in order to estimate the error associated with the calculation. It becomes obviously, therefore, that EGS will be too slow at the high energies that are now being considered. Based on these facts an alternate, less costly approach is suggested.

We will make the assumption that the $E^{-1/2}$ model is correct provided that shower containment is at a 99% level (or close to this value). A method of calorimeter design, at least for the case of sampling-type devices, would then involve:

1. determination of the dimensions (transverse and longitudinal) necessary for 99% shower containment;
2. resolution-type calculations using EGS at 1 GeV (for example) in order to determine the best sampling methods to employ;
3. following completion of (1) and (2), performing a few resolution calculations at the higher energies using EGS in order to verify that the $E^{-1/2}$ model is correct.

Items (2) and (3) are no worse than what is currently being done. Item (1), of course, presents the real difficulty which we will now address.

The new version of EGS, currently being developed by two of the authors (WRN and HH) and called EGS4, is capable of running in a non-analog mode. For example, one can introduce a relatively simple macro in the User Code that forces the "leading particle" – the one that has the highest energy in any particular interaction – to be preferentially selected over the other, therefore biasing the calculation in favor of events that are the most significant to the development of the cascade. Accordingly, in order to "play the game fairly", a weight factor must accompany the selected particle and some events must also be randomly chosen to represent the lower energy counterpart in the interaction. This "importance sampling" scheme, which has been adapted from the electromagnetic cascade program called AEGIS by Van Ginneken ([20], [16] (see Lecture 14)), is readily available in the EGS4 version and was used together with UCCAL (30 rℓ/10 mm/1 mm/10 atm) in order to study the advantages and disadvantages of the method.

In fig. 16 we plot the fraction of energy that leaks out the device as a function of the thickness. The solid curve was obtained in six standard 20 minute runs at 10 GeV using EGS3 (130 incident events/run). The closed circles were obtained using EGS4 and the leading particle scheme described above (5 runs at 2000 events/run). The EGS3 calculation took 8.62 seconds/incident as compared with 0.031 seconds/incident for EGS4, resulting in a factor of 277 increase in efficiency! The agreement between the two is extremely good. However, the error bars can be further reduced at large depths by allowing the leading particle importance sampling to be applied only in the "important" region. Namely, if we turn the scheme on during the initial 11 radiation lengths where 90% of the energy is deposited, and off for the remainder, we obtain the results shown as open circles in fig. 16. Clearly the agreement is just as good as before and the error bars are smaller. The efficiency factor compared to EGS3 has changed from 277 to 191 (0.045 seconds/incident), but it has taken fewer events to accomplish the same feat (5 runs at 600 events/run). In short, it took about 2 hours to obtain the results in fig. 16 using EGS3, but only about 2 minutes using EGS4 (i.e., EGS3 with importance sampling).

One can use this technique in order to save computer time when trying to decide on the size of the detector necessary for 99% containment. However, importance sampling techniques like this should not be used in a resolution calculation since the biasing and weighting will significantly distort the true statistical behavior [17].

7. CONCLUSIONS

Lead glass tubes with a resistive metallic surface layer provide an elegant method of constructing combined radiator and field shaping structures for drift collection calorimeters. Such structures have some advantages over conventional designs [1]. With the aid of the EGS shower program we have shown that energy resolutions that

are comparable to other gas sampling calorimeters can be achieved fairly easily. This is primarily due to the fact that the lead glass tubing restricts the path length of low energy electrons in the gas regions, thereby reducing the fluctuations. The Monte Carlo results also show that considerable improvement in the resolution will occur when the device is pressurized. The best value that we have been able to attain in our studies so far is

$$\sigma/E = (9.59 \pm 0.05)\%/E^{1/2} \ ,$$

for 10 mm (i.d.) tubes having a wall thickness of 1 mm and with a P30 gas pressure of 10 atmospheres.

EGS has also demonstrated rather graphically that the energy of the shower will have to be contained at a 98-99% level in order for the resolution to follow a $E^{-1/2}$ model. A device that is 20 radiation lengths long will contain 10 GeV showers.

Finally, we have given a receipe for the design of such calorimeters that should greatly reduce the amount of computer time required. This method uses a feature of the new EGS4 code that allows for the inclusion of importance sampling as a means of reducing the variance, thereby allowing for factors of 100 to 300 increase in efficiency for the code at 10 GeV energies. An even further increase in efficiency is expected at higher energies.

APPENDIX

CONVERSION OF THE TUBE GEOMETRY TO ALTERNATING SLABS

The tube geometry was approximated by alternating slabs of lead glass and gas regions [figs. 17(a) and 17(b)], with the effective dimensions, t_1 and t_2, chosen to give the same average cross sectional area of gas and solid material when viewed from the edge of the slabs (or tubes). Consider unit length for the x-direction. The volume of lead glass and gas inside the dotted regions are

Geometry (a):
$$V_{glass} = \pi(r_2^2 - r_1^2) \ ,$$
$$V_{gas} = \pi r_1^2 \ ,$$

Geometry (b):
$$V_{glass} = 2r_2 t_2 \ ,$$
$$V_{gas} = 2r_2 t_1 \ .$$

To effectively have the same volume of lead glass and gas we must set

$$V_{glass})_1 = V_{glass})_2 \ ,$$
$$V_{gas})_1 = V_{gas})_2 \ .$$

Therefore, we get

$$t_1 = \pi r_1^2 / 2r_2 \ ,$$
$$t_2 = \pi(r_2^2 - r_1^2)/2r_2 \ ,$$

for the slab geometry dimensions.

REFERENCES

[1] V. Perez-Mendez, A. Del Guerra, T. Mulera, H. Hirayama and W. R. Nelson, "Design of a Lead Glass Drift Calorimeter with MWPC Detection," Lawrence Berkeley Laboratory Report No. LBL-15727 (1983); to be published in the Proceedings of the Vienna Wire Chamber Conference, 15-18 February 1983.

[2] R. L. Ford and W. R. Nelson, "The EGS Code System: Computer Programs for the Monte Carlo Simulation of Electromagnetic Cascade Showers (Version 3)," Stanford Linear Accelerator Report No. SLAC-210 (1978).

[3] C. W. Fabjan and T. Ludlam, "Calorimetry in High-Energy Physics," CERN Report CERN-EP/82-37 (1982); submitted to Annual Review of Nuclear and Particle Science.

[4] S. Iwata, "Calorimeter," Nagoya University Physics Department Report No. DPNU-13-80 (1980).

[5] G. K. Lum, M. I. Green, V. Perez-Mendez and K. C. Tam, "Lead Oxide Glass Tubing Converters for Gamma Detection in MWPC," IEEE Trans. Nucl. Sci. NS-27 (1980) 157.

[6] G. K. Lum, V. Perez-Mendez and B. Sleaford, "Gamma-Ray Detection with PbO Glass Converters in MWPC: Electron Conversion Efficiency and Time Resolution," IEEE Trans. Nucl. Sci. NS-28 (1981) 821.

[7] L. E. Price, Physica Scripta 23 (1980) 685.

[8] L. E. Price, J. Dawson, D. Ayres and R. St. Denis, "Investigation of Long Drift Chambers for a Nucleon Decay Detector," IEEE Trans. Nucl. Sci. NS-29 (1982) 383.

[9] Ch. Becker, W. Weihs and G. Zech, Nucl. Instrum. Methods 200 (1982) 335.

[10] H. G. Fischer, Nucl. Instrum. Methods 156 (1978) 81.

[11] G. D. Alekseev et al., Nucl. Instrum. Methods 177 (1980) 385.

[12] M. Atac, A. V. Tollestrup and D. Potter, Nucl. Instrum. Methods 200 (1982) 345.

[13] T. A. Mulera and V. Perez-Mendez, Nucl. Instrum. Methods 203 (1982) 609.

[14] M. Conversi, Nature 241 (1973) 160.

[15] A. J. Cook and L. J. Shustek, "A User's Guide to MORTRAN 2," Stanford Linear Accelerator Center Computation Research Group Report No. CGTM-165 (1975).

[16] W. R. Nelson and T. M. Jenkins (Editors), Computer Techniques in Radiation Transport and Dosimetry (Plenum Press, New York), 1980.

[17] W. R. Nelson and H. Hirayama, "A More Efficient Way to Use EGS in the Design of High Energy Calorimeters," Stanford Linear Accelerator Center Report Number EGS User Note EUN-SLAC-22 (1983).

[18] H. Hirayama and W. R. Nelson, "EGS4 – The Landau Sampling Option (Macro)," Stanford Linear Accelerator Center Internal Report Number EGS User Note EUN-SLAC-14 (1983).

[19] R. L. Anderson, W. W. Ash, D. B. Gustavson, K. Rich, D. M. Ritson, J. R. Johnson, R. Prepost and D. E. Wiser, "Tests of Proportional Wire Shower Counter and Hadron Calorimeter Modules," IEEE Trans. Nucl. Sci. NS-25 (1978) 340.

[20] A. Van Ginneken, "AEGIS. A Program to Calculate the Average Behavior of Electromagnetic Showers," Fermilab Report FN-309 (1978).

Table I

Summary of the Results of Running EGS/UCCAL for
Several 15 Radiation Length Geometries and Gas Pressures

Gas Pressure	Tube Geometry (I.D./Wall)	Resolution (%) (1 Parameter)	Resolution (2 Parameter)
1 atm	10 mm/1 mm	$(16.34 \pm 0.45)/E^{1/2}$	$(14.59 \pm 0.74)/E^{1/2}$ $+(1.47 \pm 0.58)$
	4 mm/1 mm	$(19.00 \pm 0.26)/E^{1/2}$	$(18.21 \pm 0.89)/E^{1/2}$ $+(0.68 \pm 0.73)$
	3 mm/2 mm	$(28.16 \pm 0.35)/E^{1/2}$	$(27.01 \pm 0.93)/E^{1/2}$ $+(0.82 \pm 0.63)$
2 atm	10 mm/1 mm	$(12.90 \pm 0.94)/E^{1/2}$	$(9.14 \pm 0.48)/E^{1/2}$ $+(2.90 \pm 1.19)$
	4 mm/1 mm	$(14.69 \pm 0.40)/E^{1/2}$	$(12.90 \pm 0.15)/E^{1/2}$ $+(1.37 \pm 0.11)$
10 atm	10 mm/1 mm	$(10.00 \pm 0.34)/E^{1/2}$	$(8.54 \pm 0.20)/E^{1/2}$ $+(1.21 \pm 0.15)$
	4 mm/1 mm	$(10.64 \pm 0.45)/E^{1/2}$	$(8.55 \pm 0.43)/E^{1/2}$ $+(1.37 \pm 0.26)$

Table II

EGS3/UCCAL Computation Time Versus Energy*

Energy (GeV)	Time (seconds/incident)
1	0.863
2	1.62
4	3.23
10	8.62

* 30 rℓ/10 mm/1 mm/10 atm (using the IBM-3081).

FIGURE CAPTIONS

1. Drift calorimeter with lead glass radiator/drift tube structure and wire chamber readout.
2. EGS generated shower event in slab geometry (1 GeV/15 rℓ/10 mm/1 mm/1 atm). Charged particle and photon tracks are depicted as solid and dotted lines, respectively.
3. Same as fig. 2, but only charged particles in gas regions are shown.
4. Three dimensional plot of energy deposition (vertical scale, arbitrary units) without track length restriction and Landau sampling (1 GeV/15 rℓ/10 mm/1 mm/1 atm).
5. Same as fig. 4, but with Landau sampling included.
6. Same as fig. 4, but with both track length restriction and Landau sampling included.
7. Longitudinal shower development at 4 GeV. Comparison of measurement by Anderson [19] (solid curve) with EGS calculation (points) (15 rℓ/10 mm/1 mm/1 atm).
8. Distribution of energy deposition in gas regions for 1 GeV incident electrons (15 r*lscr*/10 mm/1 mm/1 atm).
9. Same as fig. 8, but energy is 10 GeV.
10. Energy resolution (σ/E) versus $E^{-1/2}$, showing one and two parameter straight line fits to data (15 rℓ/10 mm/1 mm/1 atm).
11. Energy resolution as a function of the inner diameter of the tubes (1 GeV/15 rℓ/1 mm walls/1 atm), for various combinations of track length restriction and Landau sampling.
12. Energy resolution versus $E^{-1/2}$ showing one parameter fit through 15 rℓ data (triangles and dashed line) and 30 rℓ data (circles and solid line) (10 mm/1 mm/10 atm). Error bars are the size of the symbols unless otherwise shown.
13. Energy resolution as a function of length of detector for 1 GeV and 10 GeV incident electrons (10 mm/1 mm/10 atm).
14. Energy resolution as a function of the fraction of energy that leaks out the back of the detector for 1 GeV and 10 GeV incident electrons (10 mm/1 mm/10 atm). Arrows indicate detector length corresponding to fig. 13.

15. Energy resolution times $E^{1/2}$ versus incident electron energy for two detector sizes (15 and 30 rℓ) (10 mm/1 mm/10 atm).
16. Fraction of energy that leaks out back of detector versus detector length (10 GeV/10 mm/1 mm/10 atm). Solid curve = normal EGS3 run (6 $\times$ 130 cases, 8.62 sec/case). Closed circles = EGS4 with biasing applied throughout (5 $\times$ 2000 cases, 0.031 sec/case). Open circles = EGS4 with biasing on for first 11 radiation lengths only (5 $\times$ 600 cases, 0.045 sec/case).
17. (a) Tube geometry and (b) alternating slab geometry.

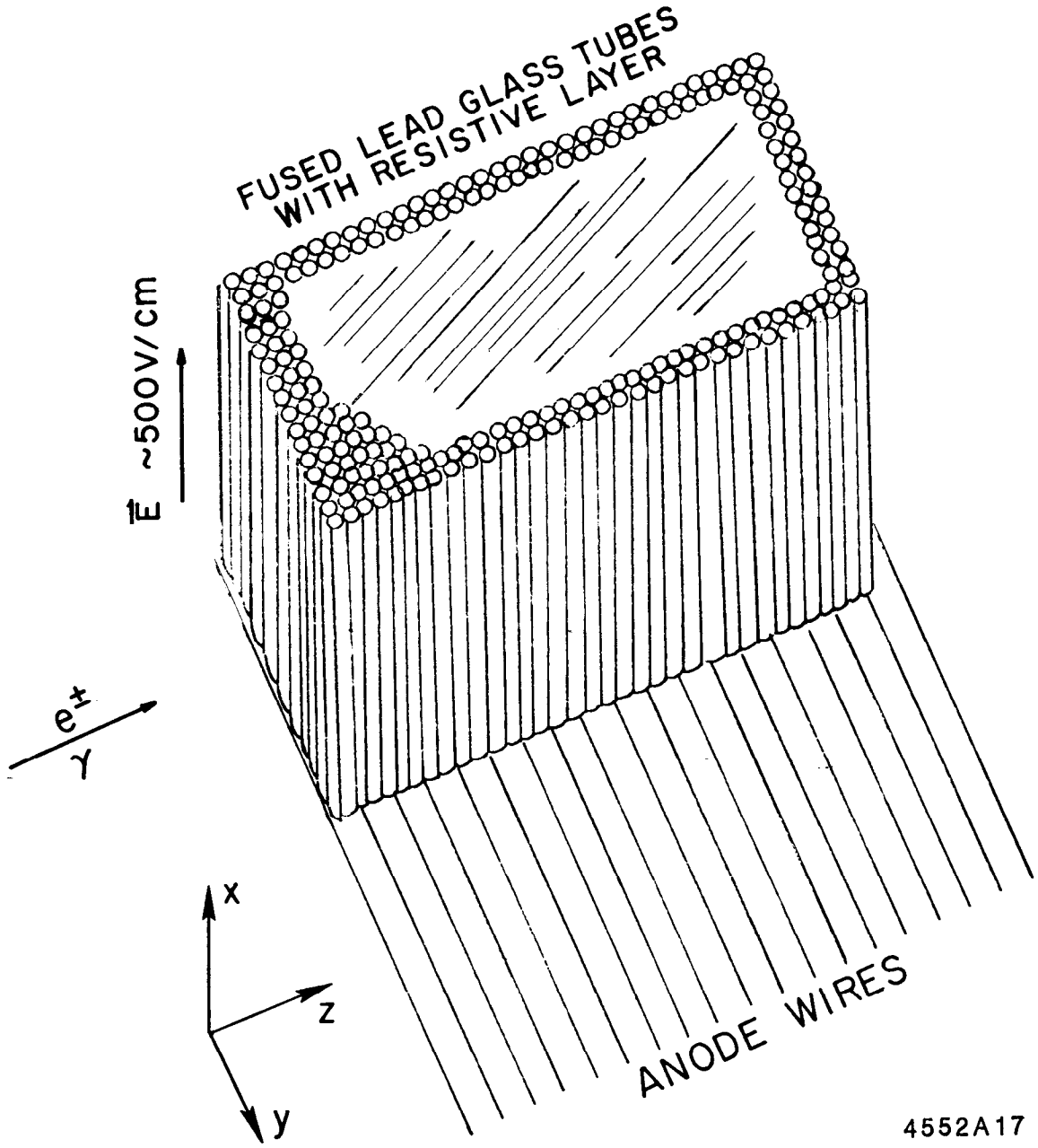
FUSED LEAD GLASS TUBES
WITH RESISTIVE LAYER
$\vec{E}$ ~500V/cm
$e^{\pm}$
γ
x
z
y
ANODE WIRES
4552A17

Fig. 1

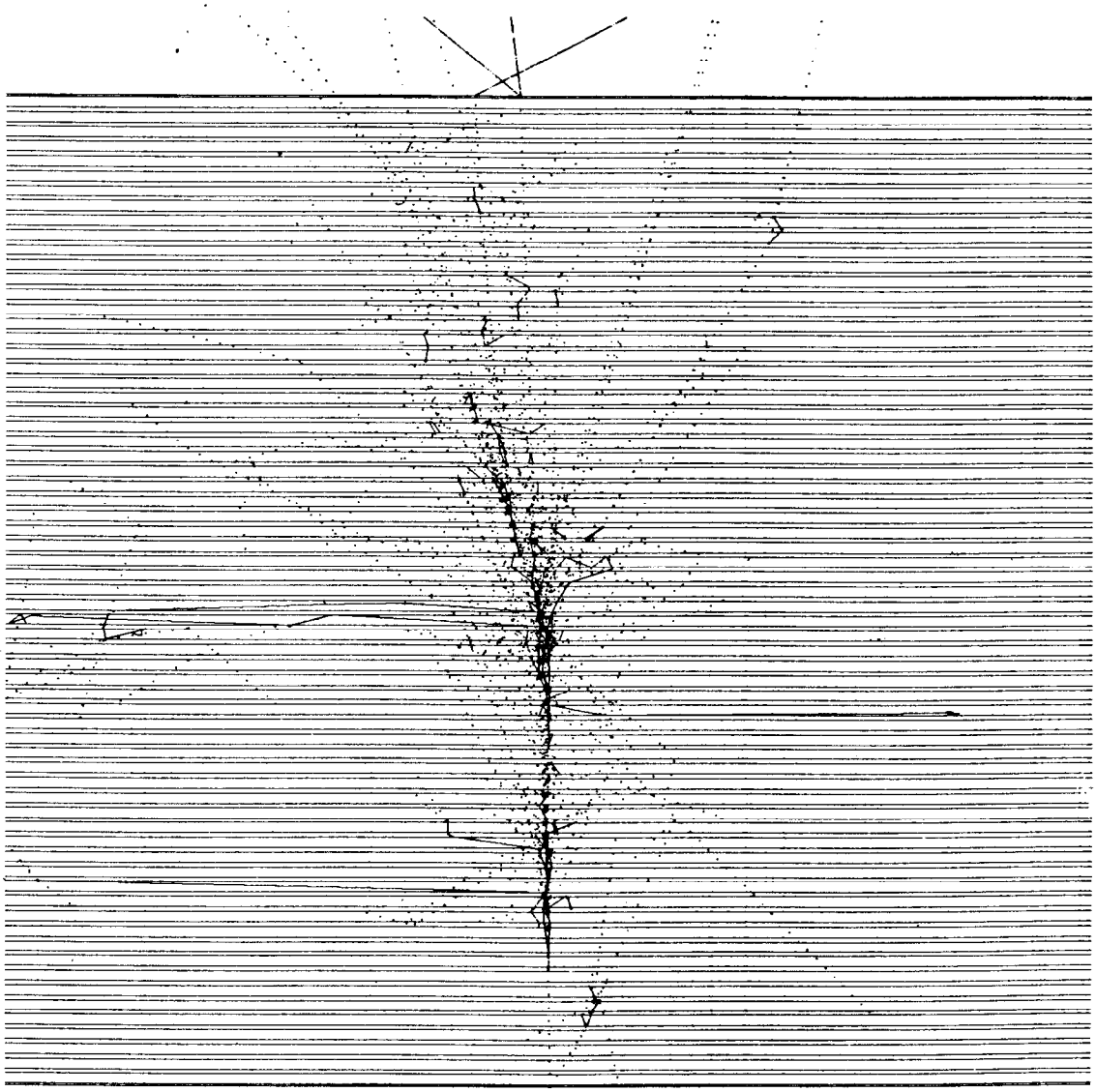

Fig. 2

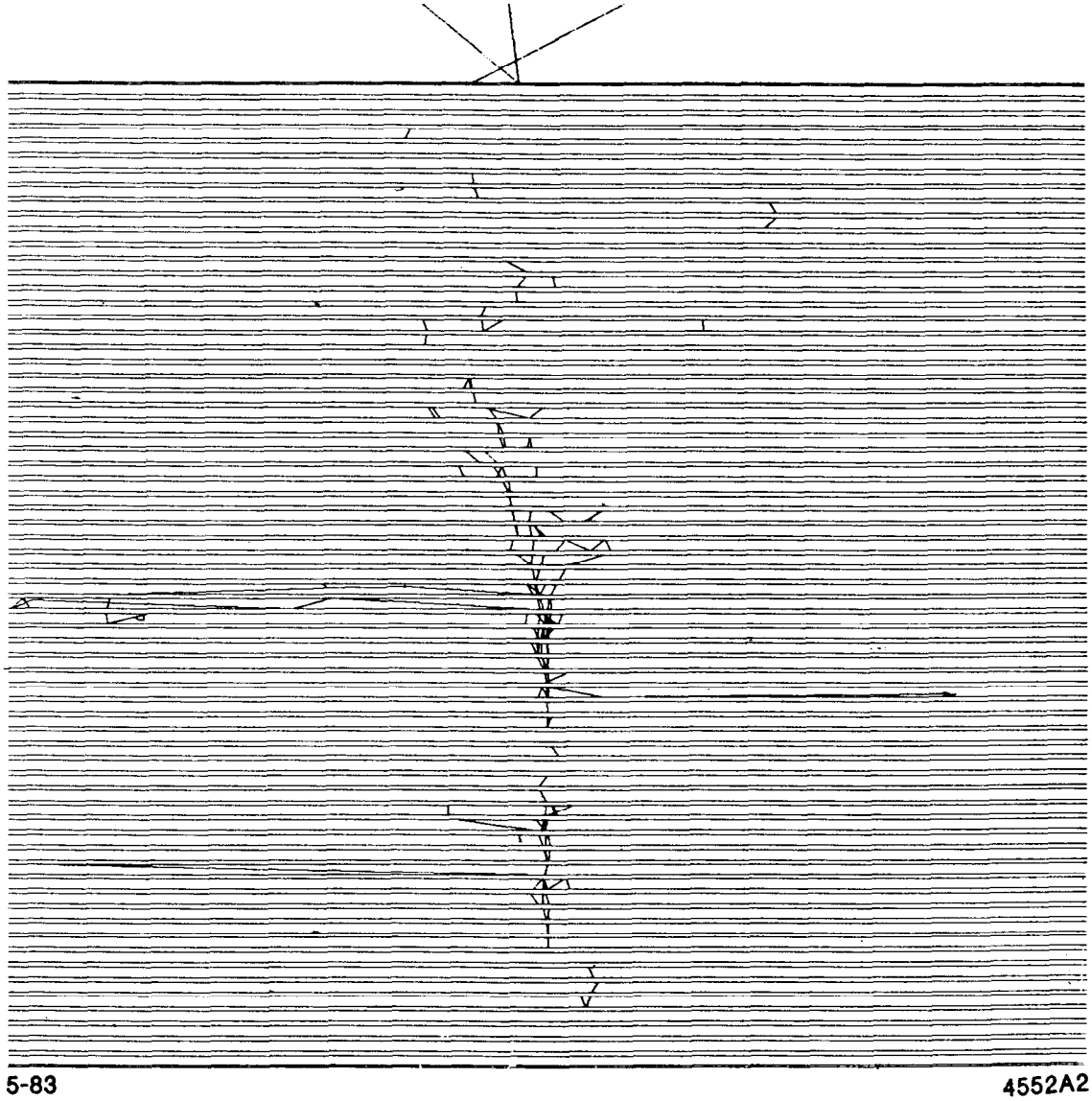

Fig. 3

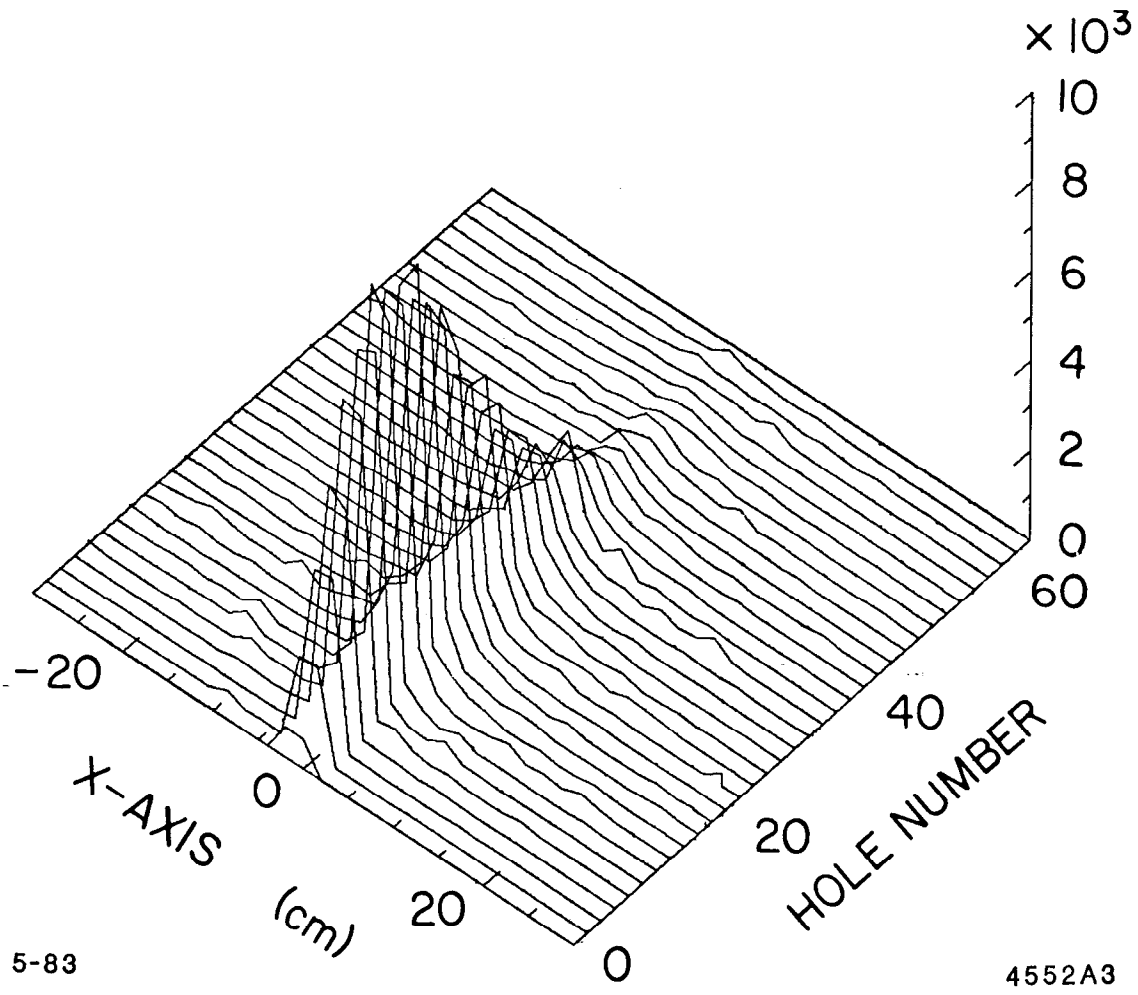

Fig. 4

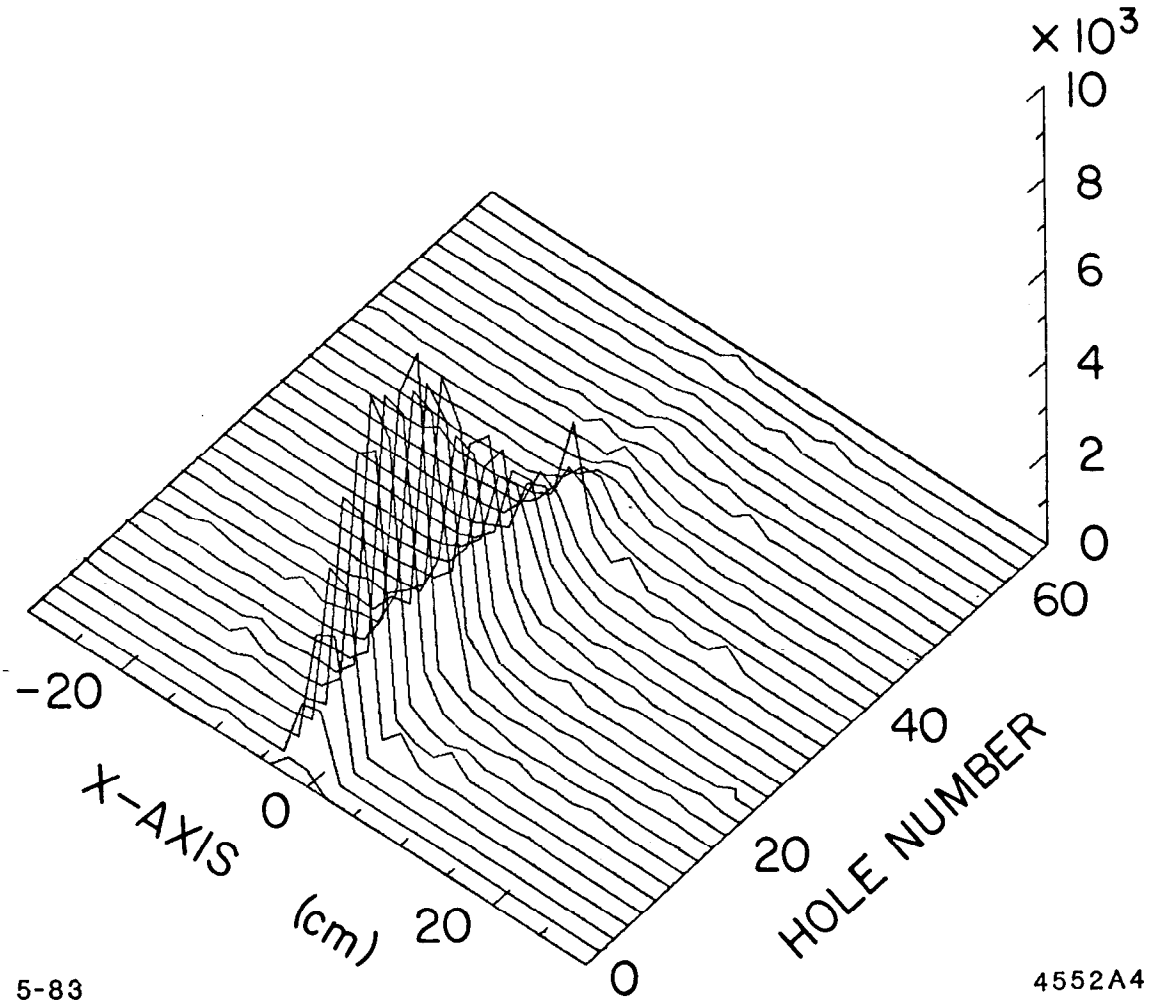

Fig. 5

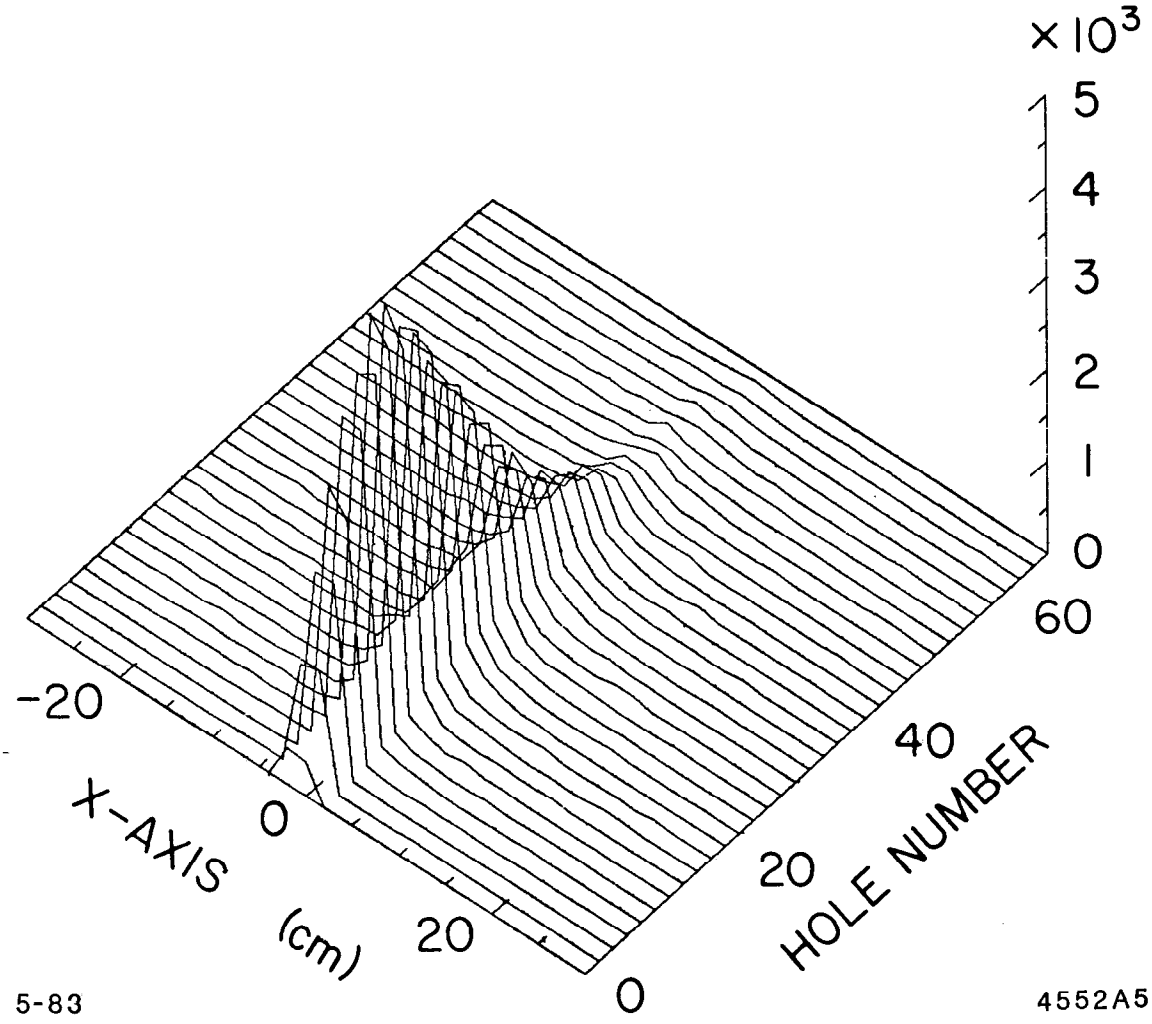

Fig. 6

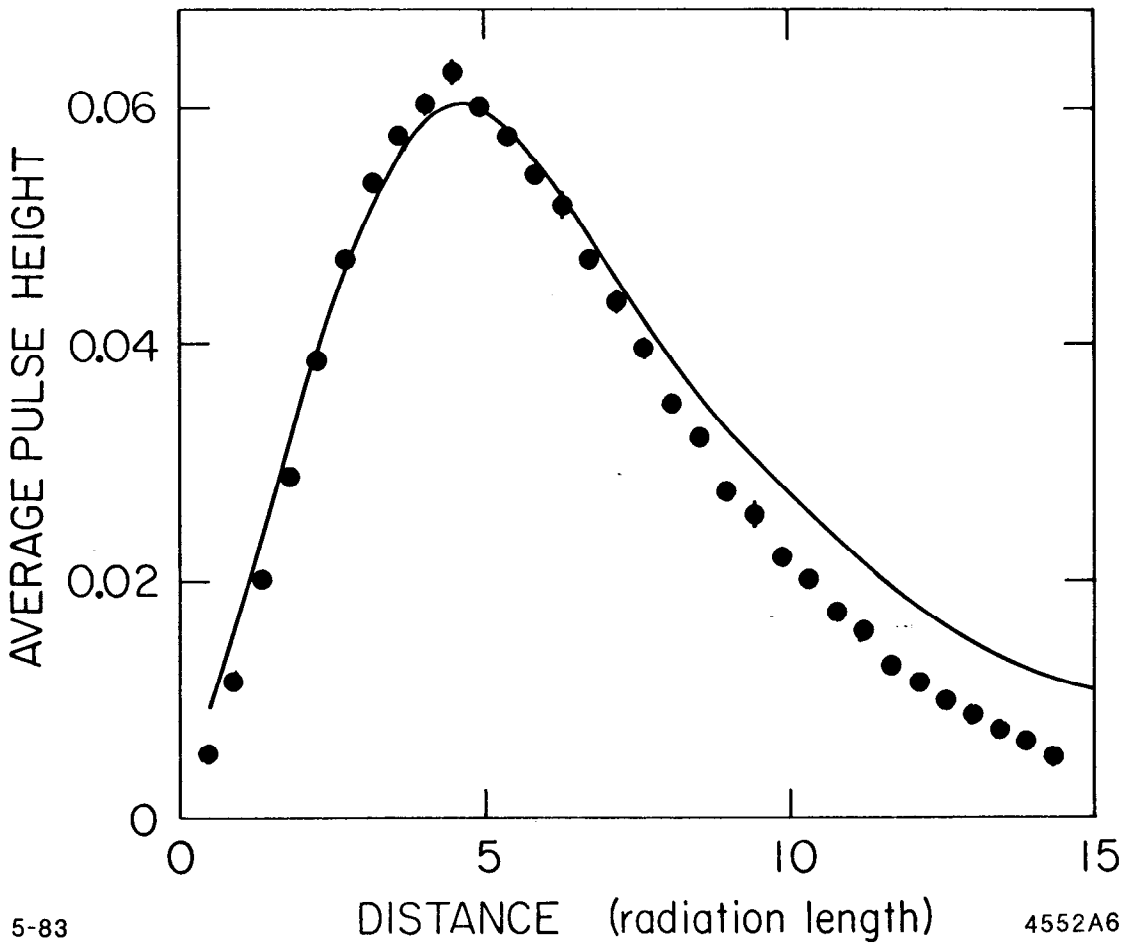
AVERAGE PULSE HEIGHT
0.06
0.04
0.02
0
0
5
10
15
DISTANCE (radiation length)
5-83
4552A6

Fig. 7

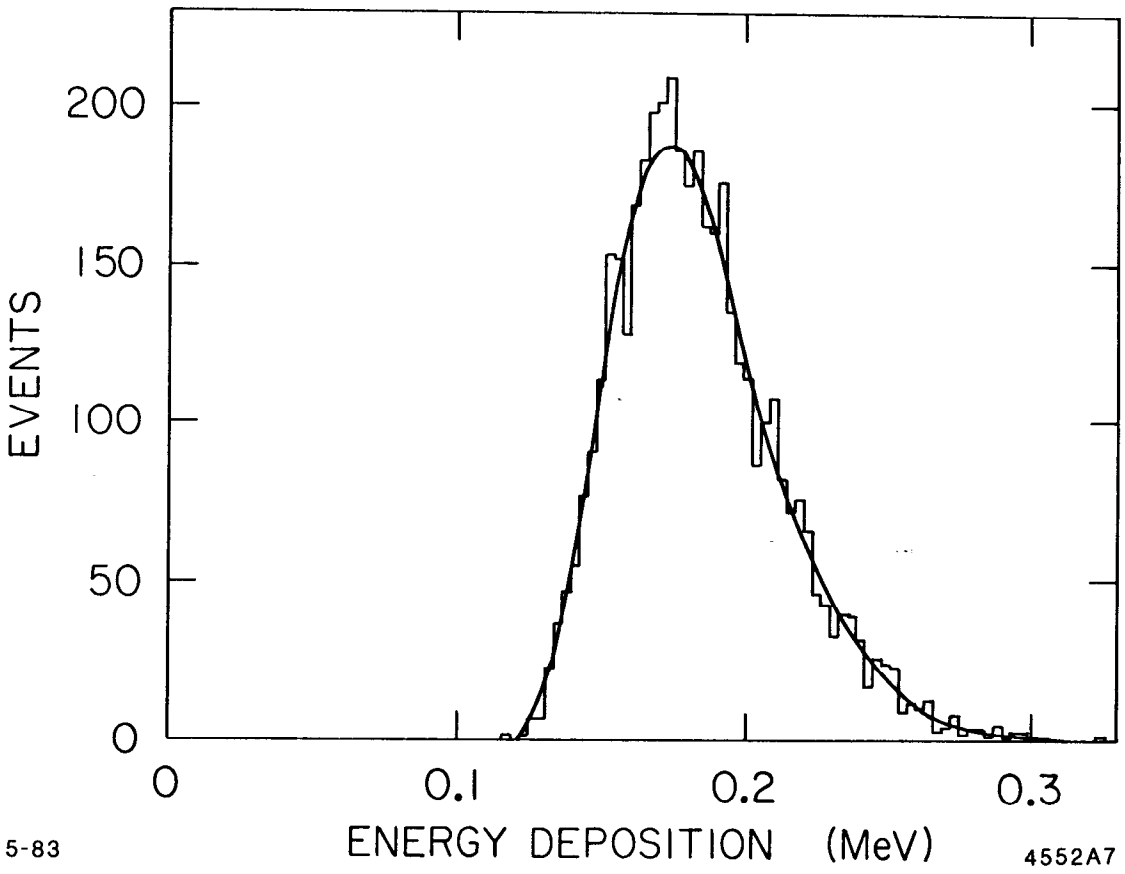
200
150
100
50
0
EVENTS
0
0.1
0.2
0.3
ENERGY DEPOSITION (MeV)
5-83
4552A7

Fig. 8

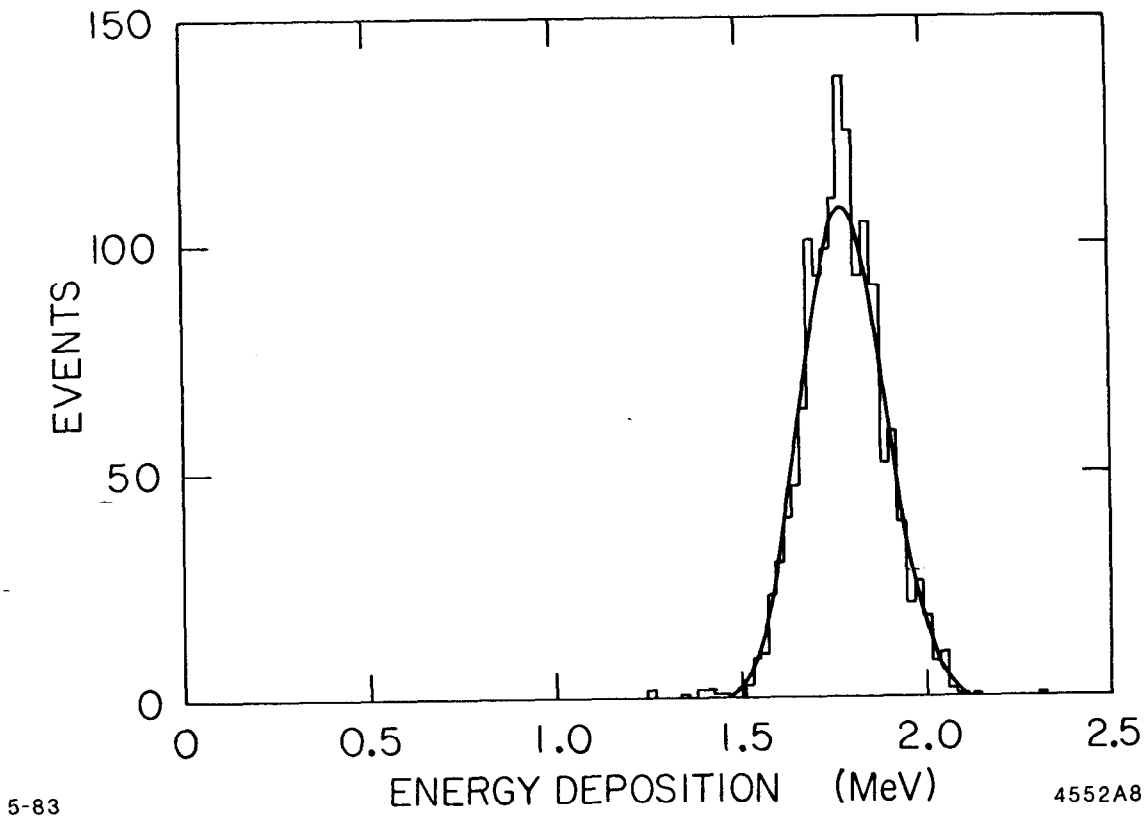
150
100
50
0
EVENTS
0
0.5
1.0
1.5
2.0
2.5
ENERGY DEPOSITION (MeV)
5-83
4552A8

Fig. 9

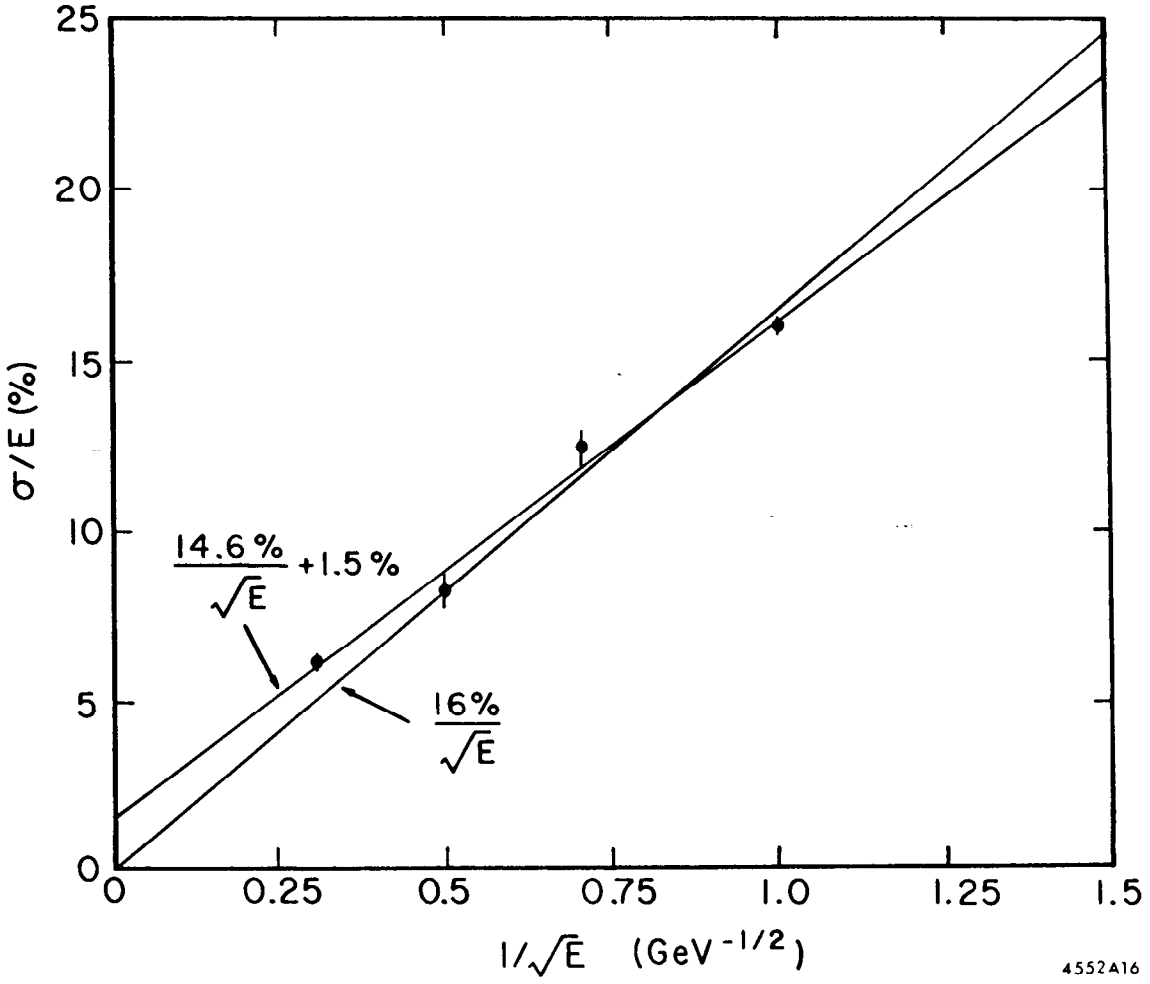
25
20
15
10
5
0
σ/E (%)
14.6 %/√E + 1.5 %
16%/√E
0
0.25
0.5
0.75
1.0
1.25
1.5
1/√E (GeV^-1/2)
4552A16

Fig. 10

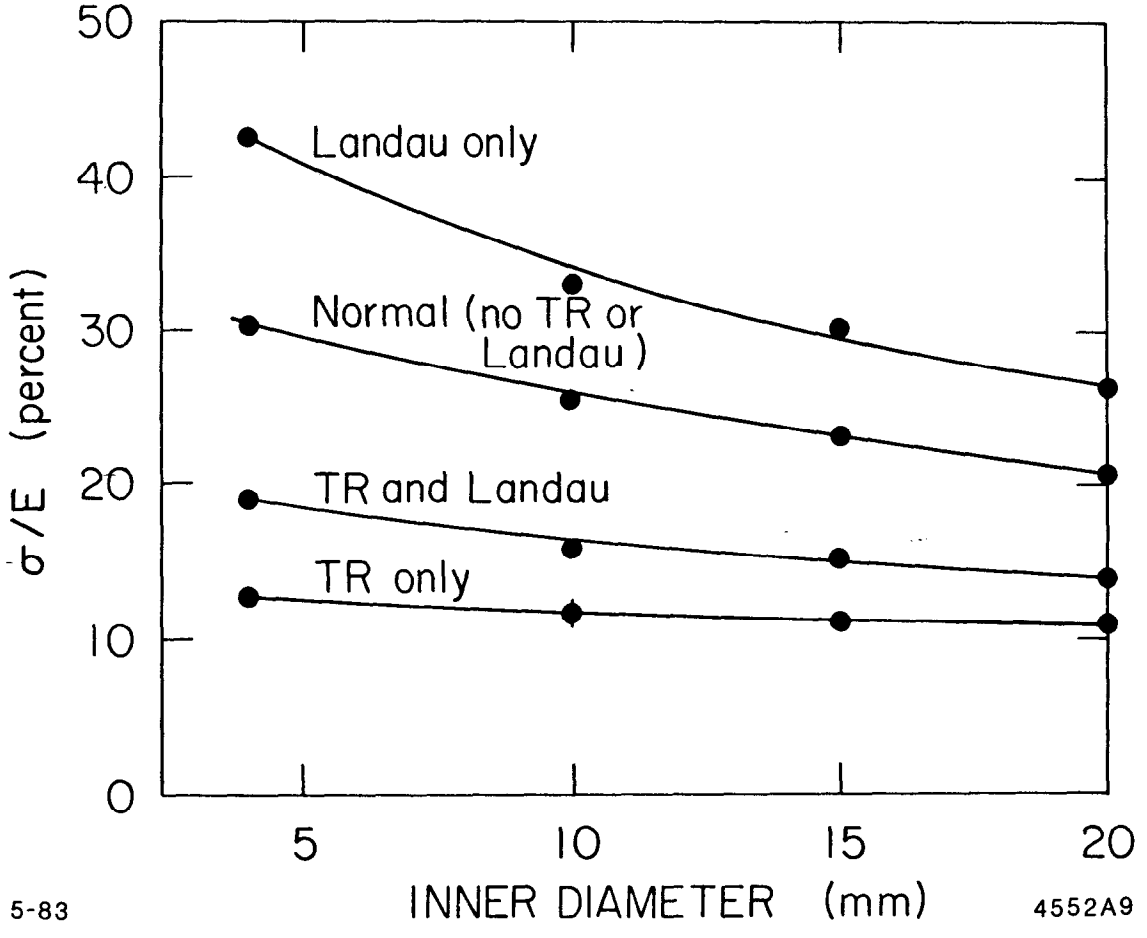
50
40
30
20
10
0
σ/E (percent)
Landau only
Normal (no TR or Landau)
TR and Landau
TR only
5
10
15
20
INNER DIAMETER (mm)
5-83
4552A9

Fig. 11

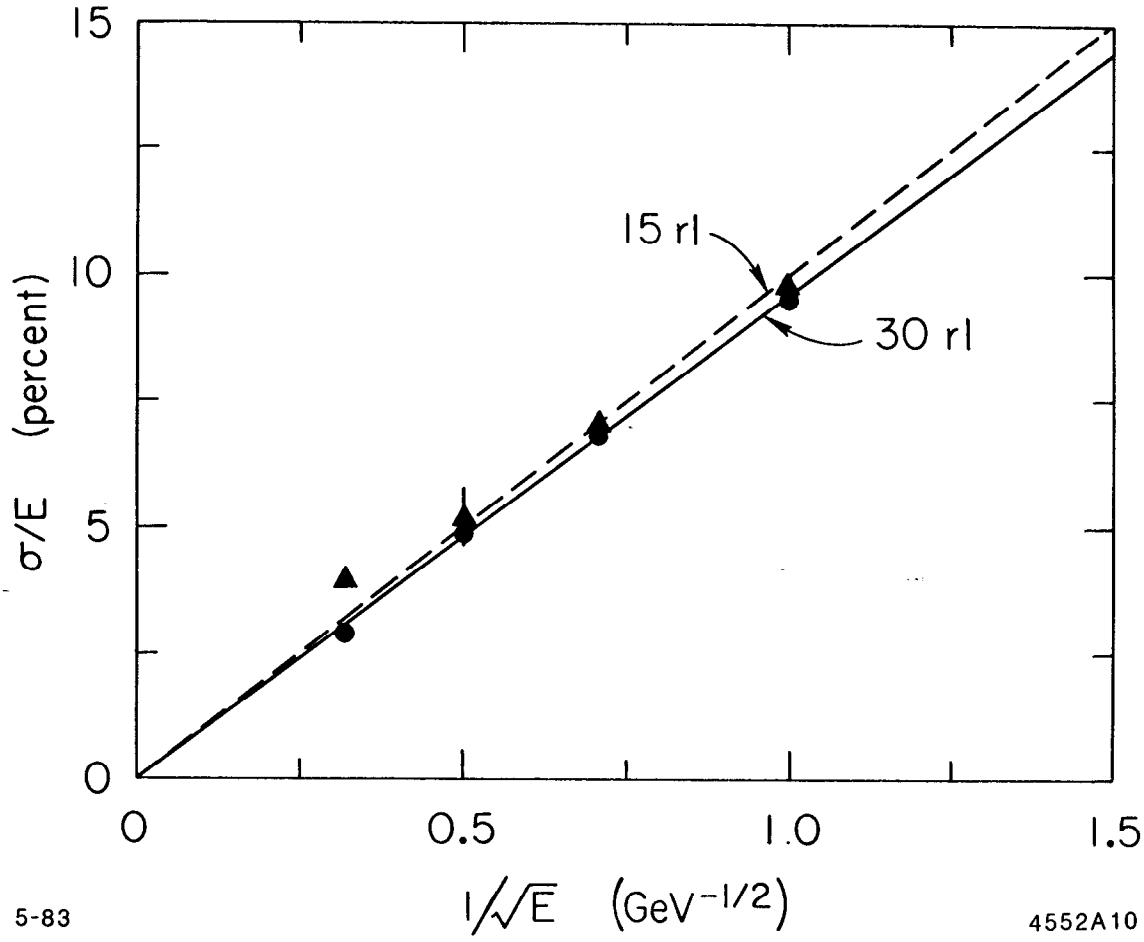

Fig. 12

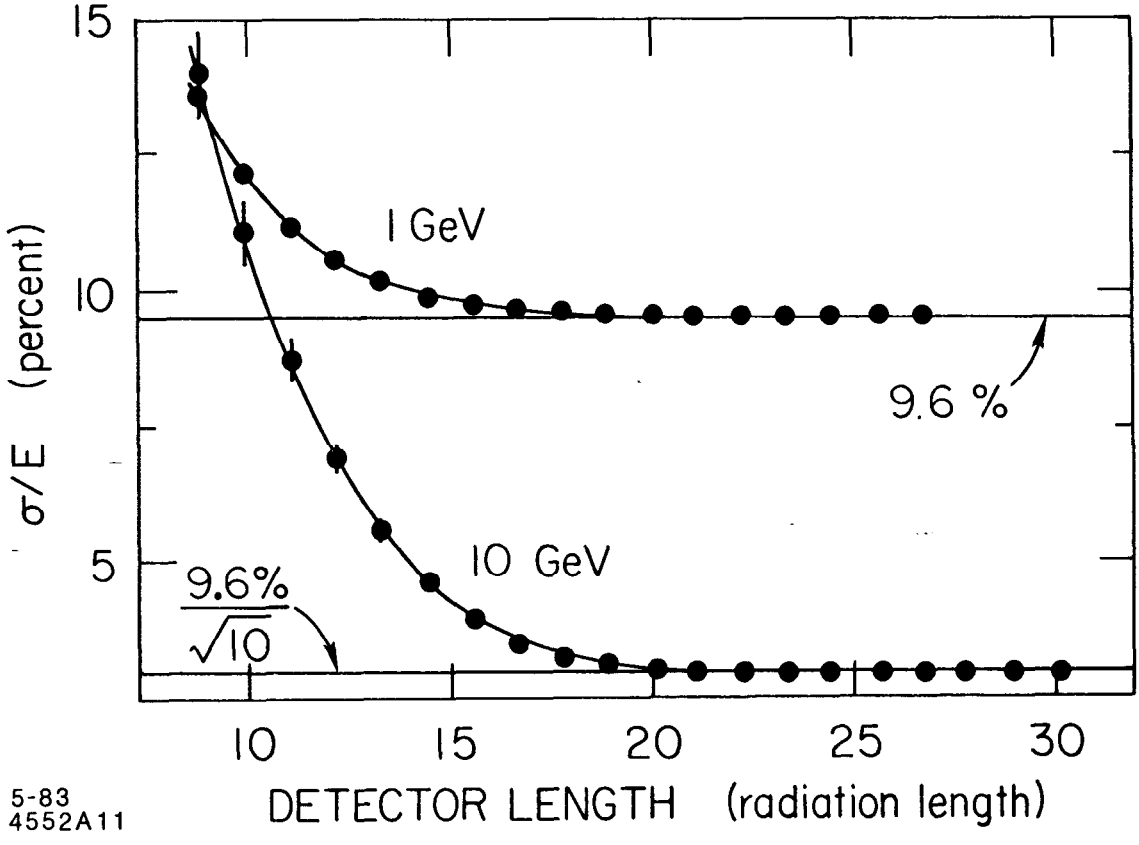
15
10
5
σ/E (percent)
1 GeV
9.6 %
10 GeV
9.6%
√10
10
15
20
25
30
DETECTOR LENGTH (radiation length)
5-83
4552A11

Fig. 13

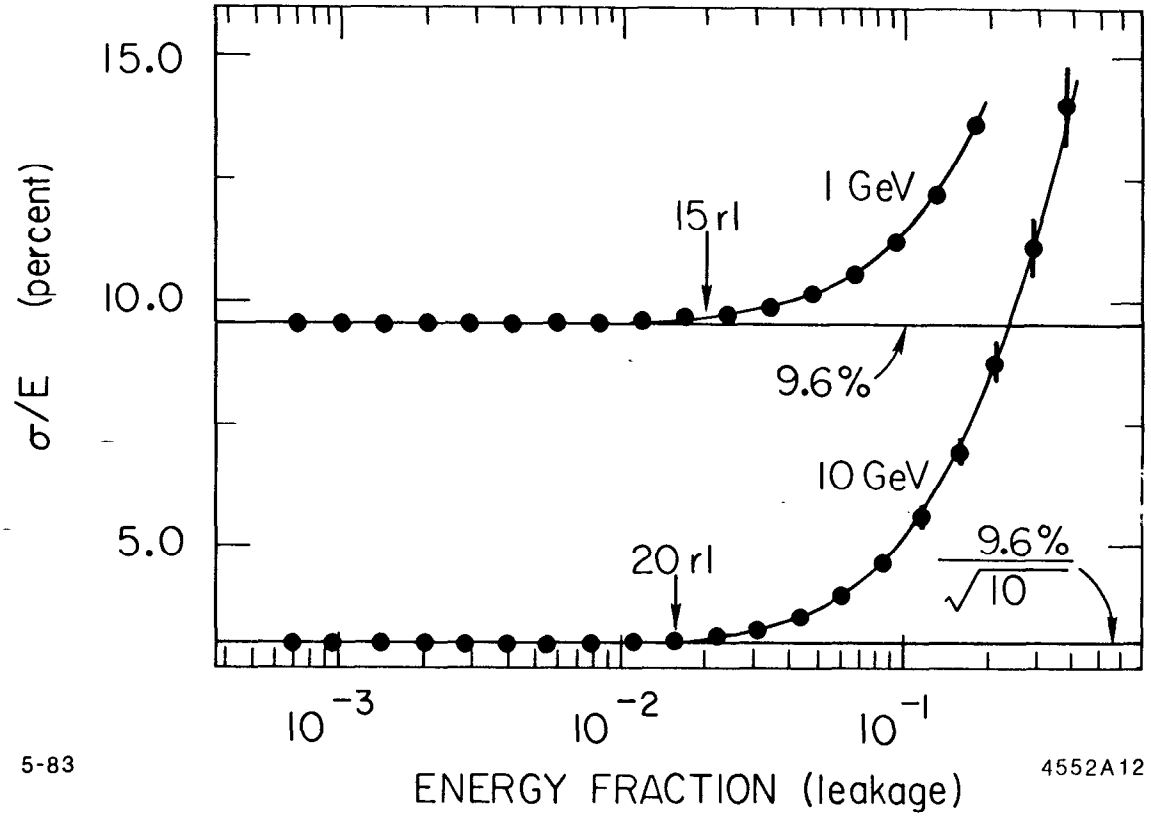
15.0
10.0
5.0
σ/E (percent)
15 rl
1 GeV
9.6%
10 GeV
20 rl
9.6%
√10
10^-3
10^-2
10^-1
ENERGY FRACTION (leakage)
5-83
4552A12

Fig. 14

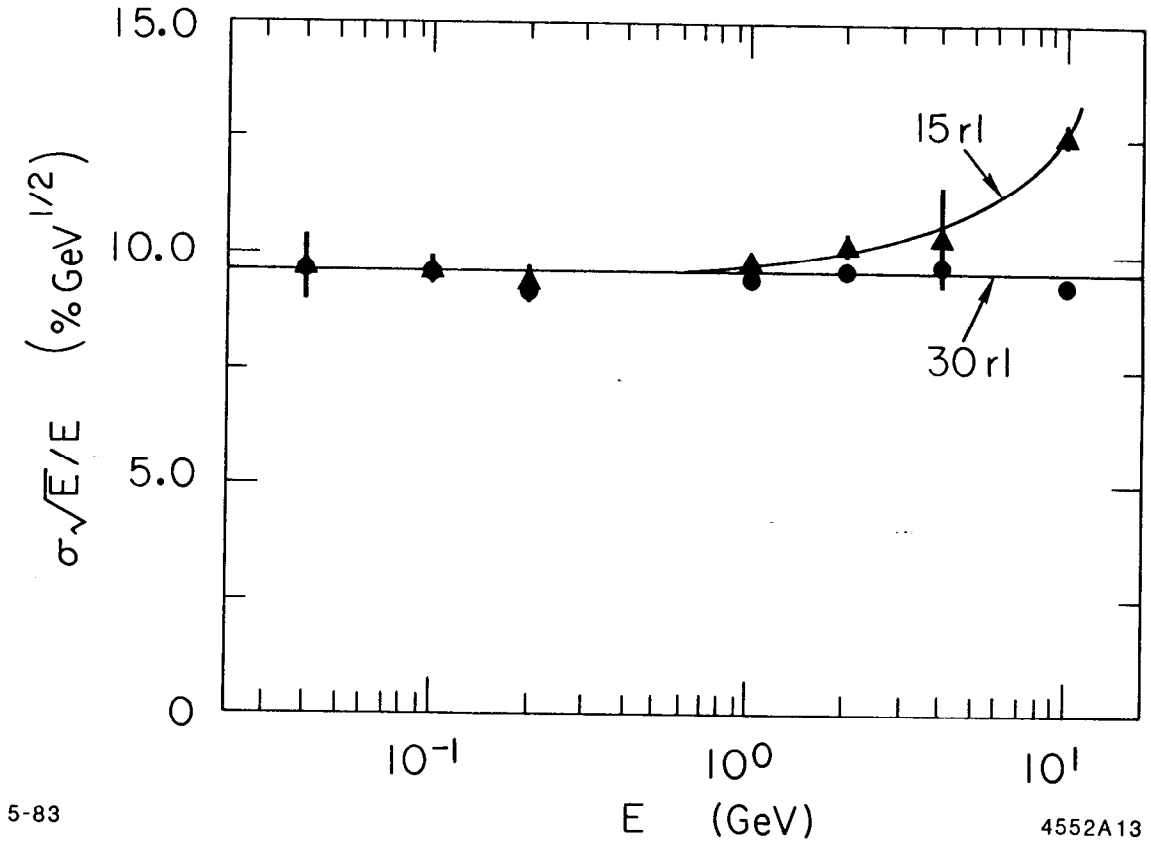
15.0
10.0
5.0
0
$\sigma\sqrt{E}/E$ (% GeV$^{1/2}$)
15 rl
30 rl
10^{-1}
10^{0}
10^{1}
E (GeV)
5-83
4552A13

Fig. 15

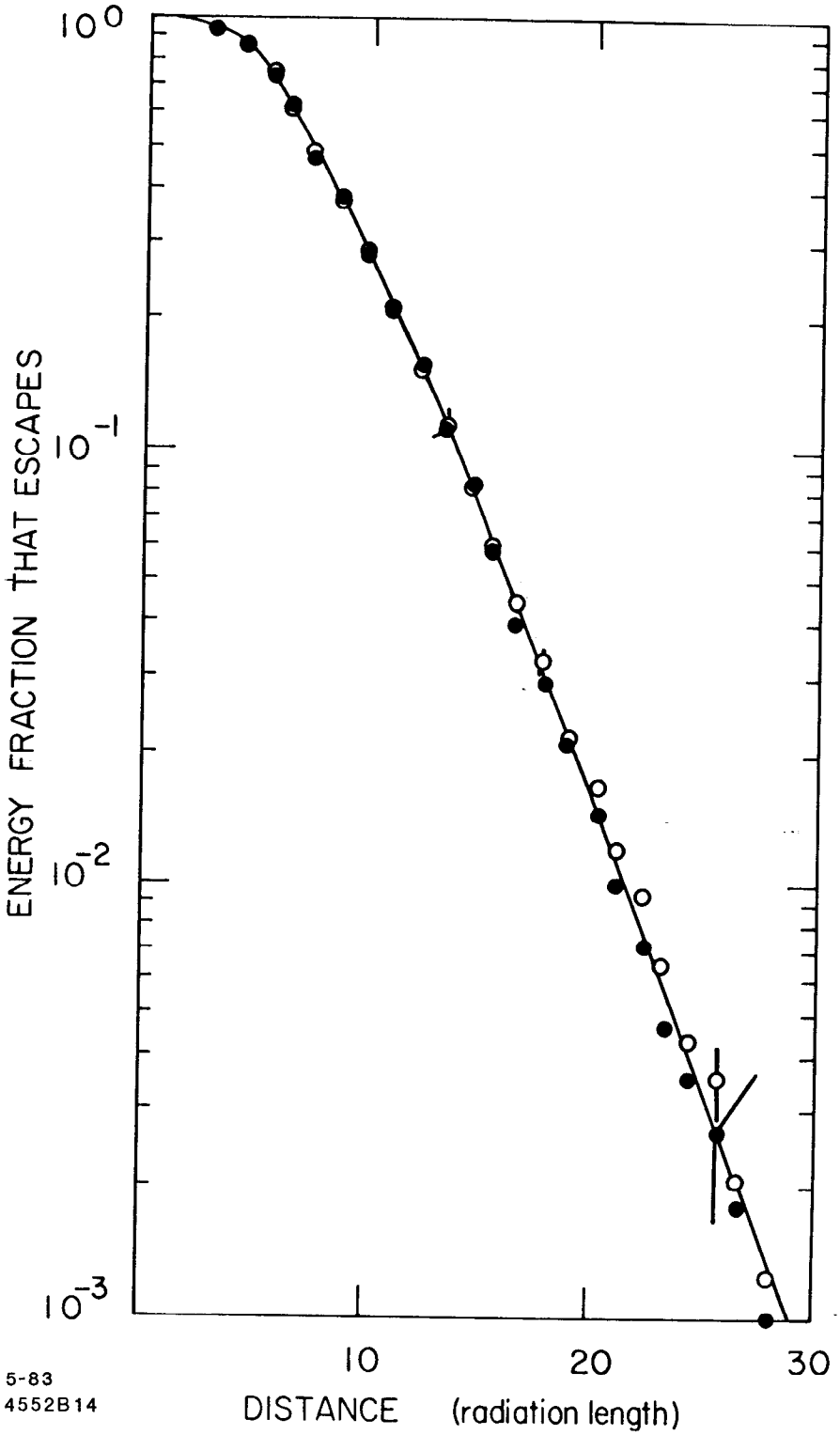
ENERGY FRACTION THAT ESCAPES
10 0
10 -1
10 -2
10 -3
10
20
30
DISTANCE (radiation length)
5-83
4552B14

Fig. 16

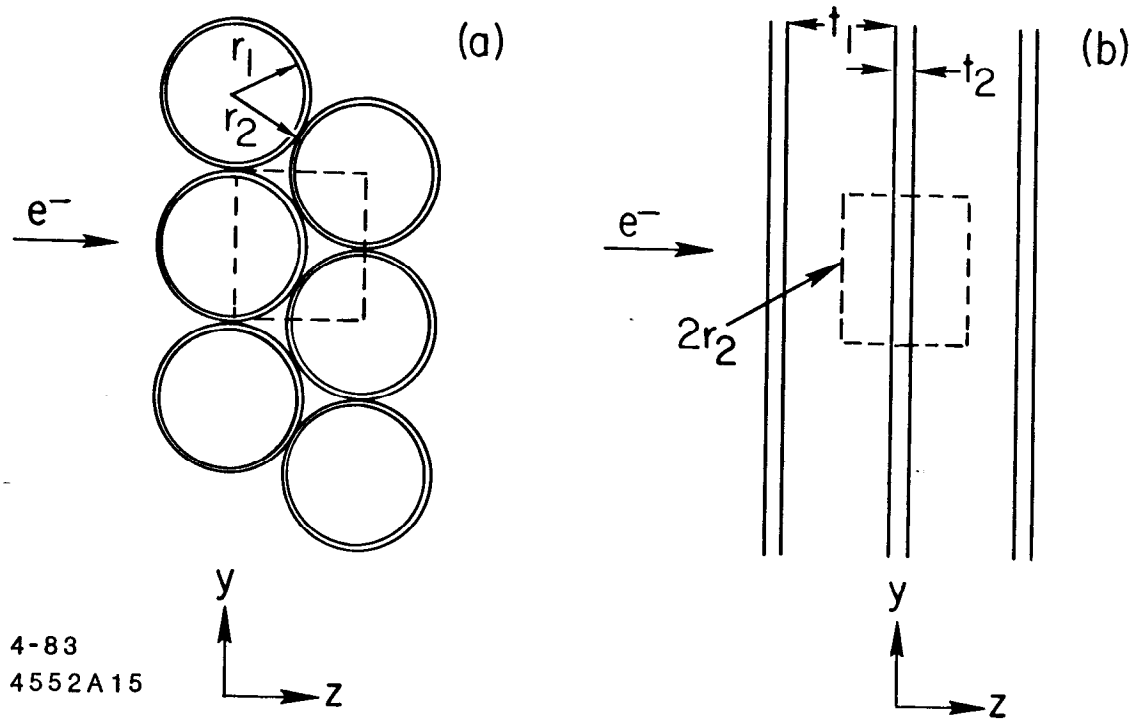

Fig. 17